Hierarchical assemblies of bismuth titanate complex architectures and their visible-light photocatalytic activities†

Jungang Hou,[ab] Yuanfang Qu,[a] Dalibor Krsmanovic,[b] Caterina Ducati,[b] Dominik Eder*[b] and R. V. Kumar*[b]

Received 6th November 2009, Accepted 7th January 2010
First published as an Advance Article on the web 11th February 2010
DOI: 10.1039/b923124b

The shape-controlled synthesis of hierarchically micro- and nanostructured materials has provided new possibilities to improve their physical and chemical properties. In this work, $Bi_{12}TiO_{20}$ complex architectures, such as nanospheres, nanowires, microflowers and microspheres were prepared through a facile solution-phase hydrothermal process, by controlling the reaction parameters, such as temperature, reagent concentration, and reaction time. Within the hydrothermal temperature range from 150 to 180 °C, the morphology transformed progressively from nanosphere agglomerates to microflowers, nanowires and then to microspheres with increasing time. A possible growth mechanism is proposed to explain the transformation of nanoparticles to microflowers *via* an Ostwald ripening mechanism followed by self-assembly and then break-up of the microflowers to nanowires and final consolidation into microspheres. Most importantly, these $Bi_{12}TiO_{20}$ samples dependent on their shape, size, and crystallinity, displayed high photocatalytic activities in comparison with bulk bismuth titanate powders, as demonstrated by the degradation of Rhodamine B under visible-light irradiation. The reasons for the difference in the photocatalytic properties of these $Bi_{12}TiO_{20}$ architectures are further investigated.

1. Introduction

Physical and chemical properties of nanomaterials depend not only on their composition but also on their structure, morphology, phase, shape, size, distribution, and spatial arrangement.[1–4] The control over morphology and size of nanostructures has become a fundamental issue in nanomaterials. Nanomaterials have attracted extensive attention as a result of their unique properties and their wide range of potential applications.[1–4] For example, development of hierarchical materials in ZnO,[5] ZnS,[6] Cu_2PO_4OH[7] and bismuth-based materials, such as Bi_2WO_6 3D structures,[8] $BiFeO_3$ pyramids and $Bi_2Fe_4O_9$ nanotubes,[9] and BiOX microspheres,[10] have been investigated. The relationship between one-dimensional (1D) structure and their evolution into self-organizing three-dimensional (3D) architectures has created much interest.[1–4] The problem of devising convenient synthesis routes to produce crystalline nanostructures, with controllable morphology using environmentally friendly protocols remains a vital challenge in nanoscale chemistry. Although various procedures have been developed, including template-based methods,[11] thermal evaporation,[12] electrochemical deposition,[13] and hydrothermal process,[14] the solution-phase synthesized route is viewed as one of the most straightforward and versatile ways for the rational design of nanostructures.

Aurivillius oxides, characterized with the general formula $Bi_2A_{n-1}B_nO_{3n+3}$ (A = Ca, Sr, Ba, Pb, Na, K, and B = Ti, Nb, Ta, Mo, W, Fe), have attracted much attention due to their layered structure and the resulting unique physical properties.[15–18] Among these, bismuth titanates, a large family that includes several phases in the Bi–Ti–O system, are promising candidates for various technological applications.[19–24] For example, Yao *et al.*[19] reported that $Bi_{12}TiO_{20}$ crystals exhibit high photocatalytic activity towards photodegradation of methyl orange under UV-light. Zhou *et al.*[20] demonstrated the potential of $Bi_{12}TiO_{20}$, as a visible-light photocatalyst for the oxidation of methanol to CO_2. Besides, $Bi_{12}TiO_{20}$ nanowires (notated as BiT NWs) and their photocatalytic activity under UV-light irradiation have been briefly reported in our previous short communication.[24] These studies revealed that BiT could perform as an excellent photocatalytic material and solar-energy-conversion material. However, to the best of our knowledge, there is no systematic study on shape control and associated visible-light photocatalytic activities of BiT.

In this work, the influences of synthesis parameters on the resulting products, the synthesis mechanism, the critical roles of treatment conditions and catalyst compositions in determining catalytic performance, as well as the contribution of the work to the fields of visible-light photocatalytic activities were not reported or elaborated in detail. Therefore, we expand on these aspects more explicitly in the current paper. There are two significant aspects of the work described in this paper. First, the synthesis of shape-controlled and homogeneous $Bi_{12}TiO_{20}$ architectures has been found to be extremely evasive to date. Hence, the low-temperature solution-phase synthesis of $Bi_{12}TiO_{20}$ architectures with well controlled shape and sizes should be an important progress that may inspire subsequent

[a]*Key Laboratory for Advanced Ceramic and Machining Technology of Ministry of Education, Tianjin University, Tianjin, 300072, China*
[b]*Department of Materials Science and Metallurgy, University of Cambridge, Cambridge, CB2 3QZ, United Kingdom. E-mail: rvk10@cam.ac.uk; Fax: +44 1223 334327; Tel: +44 1223 334467*
† Electronic supplementary information (ESI) available: Experimental details. See DOI: 10.1039/b923124b

catalytic materials synthesis. Second, catalysis by $Bi_{12}TiO_{20}$ nanoparticles has been intensively studied recently,[19–24] but the test of these $Bi_{12}TiO_{20}$ microflowers and nanowires associated optical properties and photocatalytic activities in the degradation of Rhodamine B under visible-light irradiation has been rarely reported. Hence, this work may be of interest to both materials scientists and those working in the area of catalyst design.

2. Experimental section

2.1 Synthesis

All chemicals were of analytical grade and were directly used without any treatment. In a typical procedure, stochiometric amounts of $Bi(NO_3)_3 \cdot 5H_2O$ and $Ti(OC_3H_7)_4$, a Bi/Ti ratio different with the recent work,[24] was dissolved in 10 mL of deionized water under vigorous stirring. The pH of the alkali solution was adjusted to 14 using potassium hydroxide, followed by adding a given amount of poly(vinyl alcohol) (PVA) as a capping reagent. Before being transferred to a Teflon-lined stainless autoclave (23 mL capacity), the solution mixture was prepared in an ultrasonic water bath for 30 min and kept at a filling ratio of 80% (v/v). The hydrothermal synthesis was conducted at 150–180 °C for 0–48 h in an electric oven. The system was then cooled to ambient temperature naturally. BiT complex architectures were collected and washed with distilled water and absolute alcohol several times, vacuum-dried, and kept for further characterization. Bulk bismuth titanate powder used Bi_2O_3 (Aldrich, 99.99) and TiO_2 (Aldrich, 99.99) as starting materials in the right stoichiometric ratio and then calcined at 600 °C for 2 h was also prepared by a traditional solid-state reaction for comparison with the BiT superstructures.

2.2 Characterization and photocatalytic measurements

The obtained products were characterized with X-ray diffraction (XRD) with Cu K_α radiation ($\lambda = 1.54178$ Å). SEM images were taken with a field emission scanning electron microscopy (FESEM, JEOL, JSM-6340F), transmission electron microscopy, selected area electron diffraction (TEM/SAED, CM30) operated at an accelerating voltage of 200 kV. The high resolution TEM image was acquired using a JEOL 4000EX microscopy, operated at 400 kV. The surface area of the BiT microflowers/nanowires were measured by TriStar 3000-BET/BJH Surface Area.

Photocatalytic activity was evaluated by the degradation of RhB under visible-light irradiation using a 300 W tungsten lamp with a cut-off filter ($\lambda > 400$ nm). A cylindrical Pyrex flask (200 mL) was placed in a sealed black box of which the top was open and the cut-off filter was set on the window face of the reaction vessel to ensure the desired irradiation condition. In each experiment, bismuth titanate powders as catalysts (100 mg) were added into RhB solution (1×10^{-5} M, 100 mL). Before illumination, the suspensions between photocatalyst powders and RhB at given time intervals, (3 mL aliquots) were sampled and centrifuged to remove photocatalyst powders. The filtrates were analyzed by recording the variations of the absorption-band maximum (553 nm) in the UV-vis spectrum of RhB solution using a UV-vis spectrophotometer (Perkin Elmer Lambda 850).

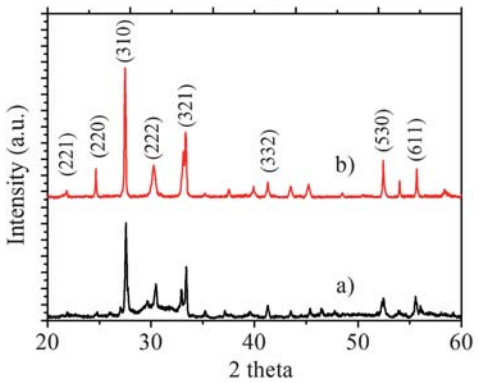

Fig. 1 XRD patterns of BiT microflowers and nanowires (0.125 mmol PVA). (a) 150 °C; (b) 180 °C for 24 h.

3. Results and discussion

3.1 Structure of $Bi_{12}TiO_{20}$ samples

Fig. 1 shows XRD patterns of the samples. Predominantly characteristic peaks can be indexed according to the BiT crystalline phase (JCPDS, Card No. 34-0097), indicating that both microflowers (150 °C/24 h) and nanowires (180 °C/24 h) are made up of BiT. The pattern (Fig. 1a) indicates that BiT microflowers are poorly crystallized. However, BiT nanowires are well-crystallized and their diffraction peaks agree well with that given in the JCPDS data file (No.34-0097). From the application point of view, the stability of a photocatalyst is important. In the case of BiT architectures, the crystal structure of the BiT architectures were very stable, as demonstrated by XRD spectra after reaction with RhB. As shown in the ESI,† the crystal structure of the photocatalyst did not change after the photocatalytic reaction.

3.2 Morphologies of architectures

3.2.1 Shape control of BiT samples. Fig. 2 shows SEM images of the samples. At 150 °C for 24 h, the micrographs indicate the presence of large spheres with diameters between 2 and 6 μm. Increasing the magnification, however, reveals that these spheres are in fact complex hierarchical architectures composed of nanowires, which appear to grow evenly from the centre of the spheres (Fig. 2b) and terminate synchronistically, so resembling flower-like structures. The magnified image at the corner in Fig. 2b shows that the diameters of the nanowires are remarkably uniform and of the order of 70–80 nm. At 180 °C for 24 h, the sample consists only of nanowires with lengths between 1 and 10 μm and diameters between 50–70 nm, which were uniform throughout their whole length (Fig. 2c,d).

Further information was obtained by TEM (Fig. 3), which confirm that the microflowers consisted of nanowires grown radially from the center. The micrographs further revealed that the diameter of the nanowires is approximately 80 nm and uniform through most of their length in the axial direction (Fig. 3a). The nanowires begin to thin out towards the end, limiting the overall size of the spherical structures to about 3 μm. The HRTEM image (Fig. 3b) reveals that the lattice spacing of a typical single-crystalline nanowire from a microflower is

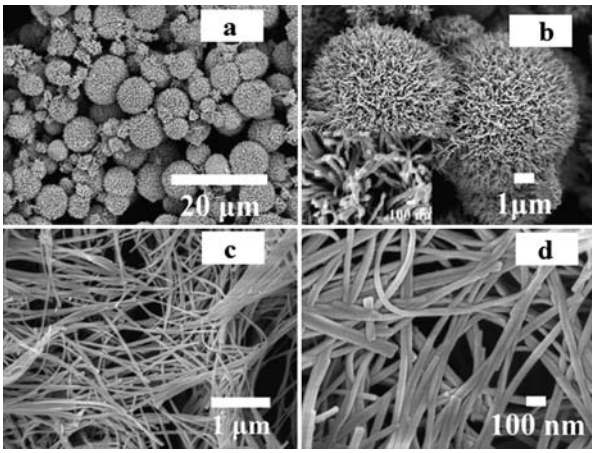

Fig. 2 SEM images of the BiT microflowers prepared at 150 °C (a,b) and 180 °C (c,d) for 24 h (0.125 mmol PVA). (a,c) Overall product morphology; (b,d) Enlarged SEM image of the flowerlike and nanowires; corresponding to a magnified image of the surface structure of an individual microflower at the corners in (b).

1.194 nm, whilst the nanoparticles with a small particle size coat the nanowires, demonstrating that the microflowers consist of single-crystalline nanowires and amorphous nanoparticles in agreement with the XRD result. Fig. 3c also presents the distribution and the mean diameter of the nanowires. The HRTEM iamge is very similar to the previous result.[24] The corresponding SAED pattern in Fig. 3d confirms the single-crystalline nature of the BiT nanowires and the corresponding ball-and-stick computer model implies a growth direction along [010].[24,25]

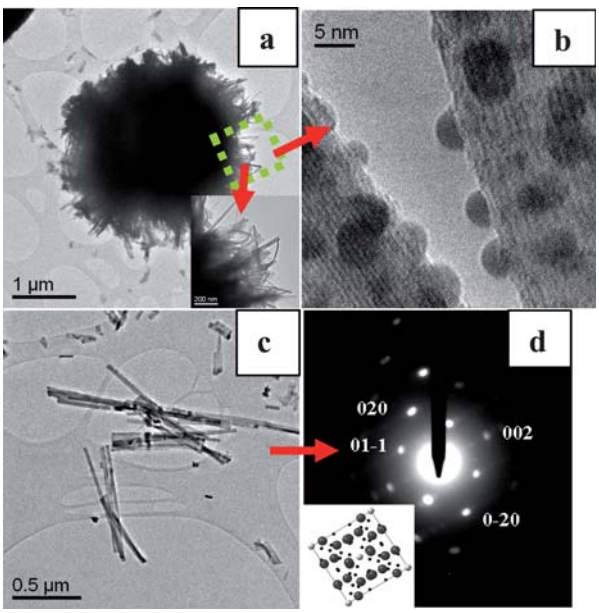

Fig. 3 TEM and HRTEM images of the BiT microflowers (a,b) and nanowires (c). (d) SAED pattern recorded from a single BiT nanowire, corresponding to the schematic representation of the crystal structure of BiT along the growth direction (Ti atoms are in light grey, Bi atoms in medium grey, O atoms in black).

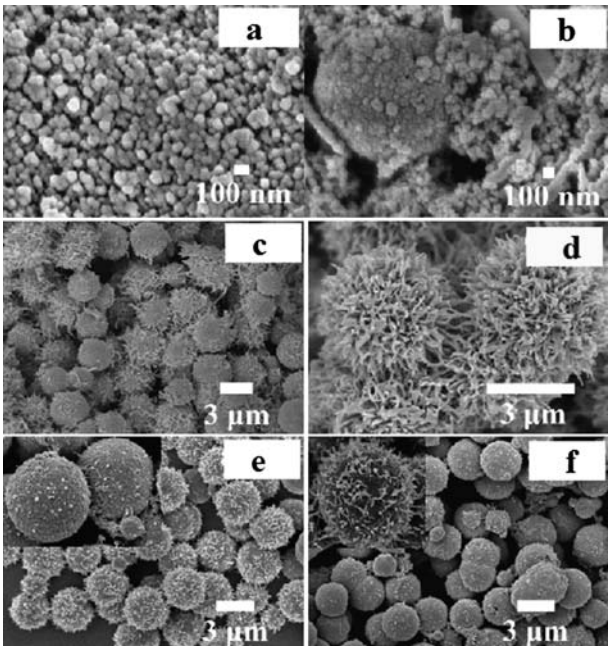

Fig. 4 SEM images of BiT samples under different conditions. At various reaction stages (a) 0 h, (b) 4 h, (c) 12 h, and (d) 24 h under the conditions (0.125 mmol PVA, 150 °C, 24 h); (e, f) at various concentrations of PVA, 150 °C, 24 h, (e) 0.075 mmol, (f) 0.15 mmol.

3.2 The effect of reaction time/PVA on morphologies

To investigate the growth mechanism of BiT architectures, the growth processes were systematically studied by analyzing the samples at different growth stages. Fig. 4a–d shows a series of SEM images of the precursor and products by varying the reaction time from 0 h to 4 h, 12 h, and 24 h at 150 °C. As shown in Fig. 4a, the precursor is composed of regular nanoparticles with a relatively small size. After 4 h of reaction, the product contains a mixture of sphere-like structures, particle aggregates, rod-like structures and dispersed nanoparticles (Fig. 4b). The regular microspheres with parts of nanowires on their surfaces obtained after 12 h (Fig. 4c). The flowery structures are constructed by lots of microspheres as the dominant products. Prolonging the reaction time to 24 h, the wire-like structures grow longer and these microspheres are assembled into the defined flower-like structures to reduce the interfacial energy of small nanocrystals (Fig. 4d).

Regarding the growth process, the presence of PVA plays an important role in affecting the morphology. As a capping reagent, PVA exhibits strong hydrogen bonding, and has often been used in the hydrothermal synthesis of nanowires, nanocables and fibers.[26–28] Based on a certain condition (0.125 mmol PVA, 150 °C, 24 h), SEM images of these samples under the various concentrations of PVA are shown in Fig. 4e and 4f. The products using 0.075 mmol PVA (Fig. 4e) are constructed by parts of nanowires growing on the microspheres, while a relatively negligible amount of nanowires was formed on the surfaces of the microsphere using 0.15 mmol PVA (Fig. 4f). Thus, the concentration of the capping reagent is the key parameter in ensuring the formation of BiT microflowers and a controlled release of this species from the solution phase to the BiT nanostructures.

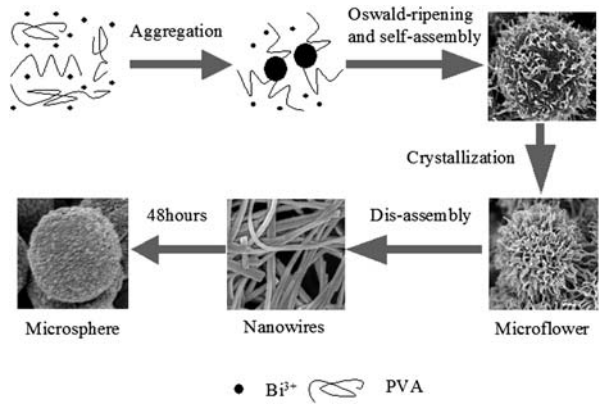

Scheme 1 Schematic illustration of the proposed formation mechanism of $Bi_{12}TiO_{20}$ microflowers/nanowires/microspheres.

3.3 Formation mechanism of $Bi_{12}TiO_{20}$ architectures

Based on the above observations, the formation mechanism of the architectures shown in Scheme 1 is proposed. In the initial stage, Bi^{3+} ions are protected by PVA molecules which can selectively adsorb onto certain surfaces, forming Bi-PVA units, and then Ti^{4+} ions can attack these units to form Bi–O–Ti precursors (step 1 in Scheme 1). After a short duration of hydrothermal treatment, sphere-like microparticles with a relatively large particle size appear through aggregation, coexisting with the nanoparticles (step 2). Microspheres with petal-like 1D structures on the surface are obtained after 12 h at 150 °C and 4 h at 180 °C (step 3) and then achieve 3D growth as the ripening time is extended and form BiT microflowers with lots of nanowires on the surface through a self-assembly process at relatively low reaction temperatures for 24 h (step 4); at high temperatures for 24 h, the microflowers that were obtained at high-temperature for 4 h (ESI†), underwent 1D growth and ripened into BiT NWs (step 5). With increasing time of hydrothermal treatment up to 36 h, the microflowers from the lower temperature broke up and transformed into microspheres (ESI†), and cubic-phase BiT NWs remain stable and a number of sphere-like structures formed as the BiT NWs joined together (ESI†). When the hydrothermal time was prolonged up to 48 h, all the samples from the low and high temperatures were evolved into microsphere-like structures as final products (ESI†). In conclusion, the evolution of the complex architectures is related to the hydrothermal treatment time rather than the temperature. Concurrently, the temperature, PVA and the dimensions of the BiT structures are summarized in Table 1. Furthermore, the capping agent plays a pivotal role in controlling the morphology of the crystals, which exhibits strong hydrogen bonding and has often been used in hydrothermal synthesis.[29,30]

Table 1 Summary of experimental results relating temperatures/T and PVA and dimensions of $Bi_{12}TiO_{20}$ nanocrystals

T/°C	Time (h)	PVA/mM	Morphology	Diameter/Length
150	24	0.075	uncomplete flowers	2–6 μm
150	24	0.125	microflowers	2–6 μm
150	24	0.15	uncomplete flowers	2–6 μm
150	0	0.125	nanoparticles	~100 nm
150	4	0.125	aggregated particles	100 nm–3 μm
150	12	0.125	uncomplete flowers	2–6 μm
150	36	0.125	microspheres	1–5 μm
150	48	0.125	microspheres	1–5 μm
180	24	0.125	long nanowires	~50 nm/1–10 μm
180	4	0.125	microflowers	1–6 μm
180	36	0.125	nanowires/microspheres	~50 nm/1–10 μm
180	48	0.125	microspheres	1–5 μm

3.4 Optical properties and photocatalytic activities

The optical properties of BiT hierarchical structures were measured using UV-Vis spectroscopy. Fig. 5A shows the diffuse reflectance spectra of the BiT samples (a: bulk powders; b: microspheres; c: microflowers; d: nanowires). Compared with bulk powders, the samples obtained by hierarchical synthesis exhibit a significant increase in photoabsorption and a shift of the absorption edge to longer wavelengths in the visible light region, indicating that all samples have potential ability for photocatalytic decomposition of organic contaminants under visible-light irradiation.

The degradation of Rhodamine B (RhB) as a representative model pollutant was chosen to evaluate the photocatalytic performance of the BiT hierarchical structures. RhB exhibits a major absorption band at 533 nm, which was followed by UV-Vis spectroscopy as a function of time upon visible light illumination (λ > 420 nm). Fig. 5B,C shows the UV-Vis spectra of the RhB solution after irradiation for various time periods in the presence of BiT microflowers and nanowires. In both cases, the irradiation caused a significant decrease of the absorption

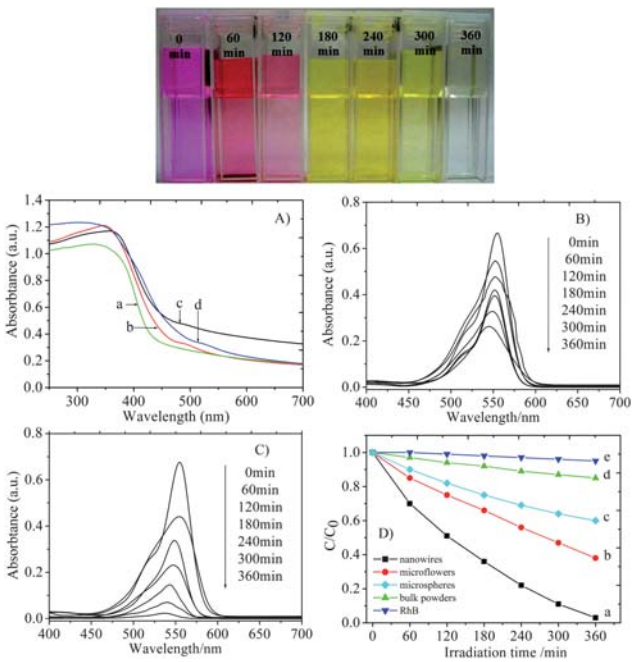

Fig. 5 (A) UV-vis reflectance spectra: (a) bulk powders, (b) microspheres, (c) microflowers and (d) nanowires; B,C) UV-visible spectral changes of RhB (1×10^{-5} M) in aqueous catalysts as a function of irradiation time under visible-light irradiation: (B) microflowers and (C) nanowires; (D) the photodegradation efficiencies of RhB as a function of irradiation time by different photocatalysts: (a) nanowires, (b) microflowers, (c) microspheres, (d) bulk powders and (e) RhB solution.

peak at 550 nm, and is associated with a diminishing of the typical purple colour of the RhB solution. Only after long reaction times, a small shift of the absorption peak towards smaller wavelength was observed. The degradation of RhB upon irradiation can proceed *via* two reactions. The oxidative attack of the aromatic part of RhB typically causes only a decrease in peak intensity, while a peak shift often accompanied by a colour change from purple to yellow is typically attributed to the diethylation of RhB.[33–36] In the present work, the decrease in the peak intensity and hence the destruction of the aromatic part was identified as the predominant process. Fig. 5D shows the kinetics of the photolysis of RhB for various BiT catalysts. In the absence of a photocatalyst, the concentration of RhB remains virtually unaffected, with only 8% of RhB being degraded after 360 min under visible-light illumination. With the addition of 100 mg of BiT as photocatalysts, the concentration of RhB decreases considerably faster, confirming BiT as an active photocatalyst for the degradation of organic pollutants in visible light. The extent of the decrease in concentration strongly depends on the morphology of the photocatalyst, with about 40%, 62% and 97% of RhB solution being decomposed after 360 min, for microspheres, microflowers and nanowires, respectively. And the microspheres obtained from the final stage (150 and 180 °C for 48 h) got the same photocatalytic activities. For comparison, the photocatalytic degradation rate of RhB over bulk BiT powder was only 15%. The differences in activity of the various BiT structures may be explained by their degree of crystallinity and their accessible surface area. The surface area according to BET was measured to be 1.4 $m^2 g^{-1}$ for the bulk sample, while the nanowires accounted for 28 $m^2 g^{-1}$. It is well known that a higher surface area increases the number of active sites and promotes the separation efficiency of the electron-hole pairs in photocatalytic reactions, resulting in a higher photocatalytic activity.[31,32] Hence, the poor photocatalytic performance of the bulk material in comparison with the other samples is attributed to its small surface area.

However, the surface area of the nanowires is rather similar to that of the microflowers (25 $m^2 g^{-1}$) and the microspheres (15 $m^2 g^{-1}$), suggesting an additional contribution based on differences in the crystallinity. The microspheres were obtained from an early stage of the synthesis (4 h). They contain polycrystalline nanoparticles and some amorphous material (Fig. 3b). In contrast, the microflowers (150 °C, 24 h) consist of single-crystalline nanowires, which have some few nanoparticles attached to their surface, which can be seen in the HRTEM (Fig. 3). The highest degree of crystallinity was found with the nanowires, which were obtained at 180 °C after 24 h. The degree of crystallinity plays a crucial role in the photocatalytic performance of catalysts.[31,32] Defects can act as scattering centres, promoting the recombination of electron-hole pairs and so limiting the photocatalytic activity.[33–36] The differences in activity between the microspheres and the microflowers and nanowires is thus a combination of increased specific surface area and a higher degree of crystallinity. Nanowires are more active than microflowers, but have a similar degree of crystallinity (TEM). BET surface areas are similar, but the surface area accessible to the large RhB molecules may be lower in the microflowers due to diffusion limitations. Whereas the nanowires are open structures that allow nearly complete access to the whole BET surface area.

4. Conclusion

In summary, BiT complex architectures were prepared through a hierarchical synthesis route in binary aqueous solution. The novelty of this work is summarized as follows:

(1) Besides nanowires, 3D microflowers were fabricated for the first time by simply controlling the solution-phase reaction parameters, such as the temperature, reagent concentration, and the reaction time.

(2) Systematic studies on the synthesis of nanospheres-microflowers-nanowires-microspheres were conducted and a possible growth mechanism is proposed to explain the transformation of nanoparticles to microflowers *via* an Ostwald ripening mechanism followed by self-assembly and then break-up of the microflowers to nanowires and finally consolidation into microspheres.

(3) Most importantly, these $Bi_{12}TiO_{20}$ microflowers and nanowires exhibited shape-associated optical properties and photocatalytic activities in the degradation of Rhodamine B under visible-light irradiation for the first time, demonstrating higher photocatalytic activities in comparison with the bulk bismuth titanate powders.

Thus, this work not only provides an example of shape-dependent photocatalytic properties of bismuth titanate but also opens up new possibilities in designing ideal building blocks of binary materials for future applications.

Acknowledgements

This work was supported in part by EPSRC and PCME Ltd. The authors gratefully acknowledge the CSC (China Scholarship Council), Government of People's Republic of China, for providing financial assistance.

References

1 J. T. Hu, T. W. Odom and C. M. Lieber, *Acc. Chem. Res.*, 1999, **32**, 435.
2 J. Goldberger, R. Fan and P. D. Yang, *Acc. Chem. Res.*, 2006, **39**, 239.
3 M. P. Zach, K. H. Ng and R. M. Penner, *Science*, 2000, **290**, 2120.
4 X. B. Cao, Y. Xie and L. Y. Li, *Adv. Mater.*, 2003, **15**, 1914.
5 F. Lu, W. P. Cai and Y. G. Zhang, *Adv. Funct. Mater.*, 2008, **18**, 1047.
6 S. L. Xiong, B. J. Xi, C. M. Wang, D. C. Xu, X. M. Feng, Z. C. Zhu and Y. T. Qian, *Adv. Funct. Mater.*, 2007, **17**, 2728.
7 I. S. Cho, D. W. Kim, S. Lee, C. H. Kwak, S. T. Bae, J. H. Noh, S. H. Yoon, H. S. Jung, D. W. Kim and K. S. Hong, *Adv. Funct. Mater.*, 2008, **18**, 2154.
8 L. S. Zhang, W. Z. Wang, L. Zhou and H. L. Xu, *Small*, 2007, **3**, 1618.
9 J. T. Han, Y. H. Huang, X. J. Wu, C. L. Wu, W.W, B. Peng, W. Huang and J. B. Goodenough, *Adv. Mater.*, 2006, **18**, 2145.
10 X. Zhang, Z. H. Ai, F. L. Jia and L. Z. Zhang, *J. Phys. Chem. C*, 2008, **112**, 747.
11 S. N. Mlondo, E. M. Andrews, P. J. Thomas and P. O'Brien, *Chem. Commun.*, 2008, 2768.
12 J. Y. Lao, J. Y. Huang, D. Z. Wang and Z. F. Ren, *Nano Lett.*, 2003, **3**, 235.
13 G. R. Li, C. Z. Yao, X. H. Lu, F. L. Zheng, Z. P. Feng, X. L. Yu, C. Y. Su and Y. X. Tong, *Chem. Mater.*, 2008, **20**, 3306.
14 Y. S. Ding, X. F. Shen, S. Gomez, H. Luo, M. Aindow and S. L. Suib, *Adv. Funct. Mater.*, 2006, **16**, 549.
15 K. R. Kendall, C. Navas, J. K. Thomas and H. C. zur Loye, *Chem. Mater.*, 1996, **8**, 642.

16 Y. Tsunoda, M. Shirata, W. Sugimoto, Z. Liu, O. Terasaki, K. Kuroda and Y. Sugahara, *Inorg. Chem.*, 2001, **40**, 5768.
17 J. Y. Kim, I. Chung, J. H. Choy and G. S. Park, *Chem. Mater.*, 2001, **13**, 2759.
18 Y. Tsunoda, W. Sugimoto and Y. Sugahara, *Chem. Mater.*, 2003, **15**, 632.
19 W. F. Yao, H. Wang, X. H. Xu, X. F. Cheng, J. Huang, S. X. Shang, X. N. Yang and M. Wang, *Appl. Catal., A*, 2003, **243**, 185.
20 J. K. Zhou, Z. G. Zou, A. K. Ray and X. S. Zhao, *Ind. Eng. Chem. Res.*, 2007, **46**, 745.
21 J. G. Hou, R. V. Kumar, Y. F. Qu and D. Krsmanovic, *J. Nanopart. Res.*, 2009, 11, DOI: 10.1007/s11051-009-9624-z.
22 L. D. Kong, H. H. Chen, W. M. Hua, S. C. Zhang and J. M. Chen, *Chem. Commun.*, 2008, 4977.
23 W. F. Su and Y. T. Lu, *Mater. Chem. Phys.*, 2003, **80**, 632.
24 J. G. Hou, Y. F. Qu, D. Krsmanovic, C. Ducati, D. Eder and R. V. Kumar, *Chem. Commun.*, 2009, 3937.
25 W. Wei, Y. Dai and B. B. Huang, *J. Phys. Chem. C*, 2009, **113**, 5658.
26 Y. J. Zhan and S. H. Yu, *J. Am. Chem. Soc.*, 2008, **130**, 5650.
27 L. B. Luo, S. H. Yu, H. S. Qian and J. Y. Gong, *Chem. Comm.*, 2005, **7**, 793.
28 X. Y. Zhang, L. Bourgeois, J. F. Yao, H. T. Wang and P. A. Webley, *Small*, 2007, **3**, 1523.
29 J. T. Han, Y. H. Huang, X. J. Wu, C. L. Wu, W. Wei, B. Peng, W. Huang and J. B. Goodenough, *Adv. Mater.*, 2006, **18**, 2145.
30 Y. Chang and H. C. Zeng, *Cryst. Growth Des.*, 2004, **4**, 397.
31 W. W. Wang, Y. J. Zhu and L. X. Yang, *Adv. Funct. Mater.*, 2007, **17**, 59.
32 F. Amano, A. Yamakata, K. Nogami, M. Osawa and B. Ohtani, *J. Am. Chem. Soc.*, 2008, **130**, 17650.
33 A. Sclafani, L. Palmisano and M. Schiavello, *J. Phys. Chem.*, 1990, **94**, 829.
34 J. Tang, Z. Zou and J. Ye, *Angew. Chem., Int. Ed.*, 2004, **43**, 4463.
35 A. T. Bell, *Science*, 2003, **299**, 1688.
36 W. Z. Wang, W. Zhu and H. L. Xu, *J. Phys. Chem. C*, 2008, **112**, 16754.